JOURNAL OF MATERIALS SCIENCE 32 (1997) 3675–3685

Deformation of spherulitic polyethylene thin films

M. F. BUTLER, A. M. DONALD*
Department of Physics, Cavendish Laboratory, University of Cambridge, Madingley Road, Cambridge, CB3 0HE, UK

Thin spherulitic films of polyethylene (PE), made by casting from xylene solution, were deformed on copper grids and their deformation microstructure studied using optical and transmission electron microscopy. A range of molecular weights, branch amounts and types, and thermal histories was used to study the influence of sample microstructure on the deformation behaviour. The spherulite boundaries were the weakest regions of spherulitic structures in all types of PE. Higher strains were generally required to deform the interiors of spherulites, which deformed by a different mechanism. The toughness of the films was increased by increasing the tie-molecule density and disentanglement resistance, to strengthen spherulite boundaries. Three methods for increasing the toughness were demonstrated and were: (1) decreasing the crystallization time in order to increase the tie-molecule density, (2) increasing the molecular weight in order to increase the tie-molecule density, and (3) incorporating short-chain branches on the main chains in order to increase the tie-molecule density and increase the disentanglement resistance. Incorporation of short-chain branches was shown to be the most effective way of strengthening spherulitic structures, with the toughest films being those made of branched PE that had been crystallized rapidly. The branch length and spherulite size were found to be unimportant.

1. Introduction

Polyethylene (PE) is a semi-crystalline thermoplastic composed of crystalline (orthorhombic unit cell [1]) lamellae surrounded by amorphous interlamellar material. The lamellae usually aggregate radially from a sheaf-like central structure to form structures known as spherulites, illustrated in Fig. 1 [2].

Thermal stresses during crystallization may cause the lamellae to become twisted. Lamellae are usually a few tens of nanometres thick and spherulites reach diameters of tens of micrometres. Some molecules are incorporated into more than one lamella; they are known as "tie molecules" and are of central importance in determining the mechanical properties of PE [3]. The extent of the tie-molecule network depends upon both the molecular weight and the long spacing (lamellar plus interlamellar thickness), because a tie molecule can be formed if the end-to-end distance of a molecule exceeds twice the lamellar thickness plus the interlamellar thickness [4]. The longer the molecules and the smaller the long spacing, the more likely it is that tie molecules, will form. Control over the long spacing may be achieved by altering the crystallization conditions [5] and by the inclusion of branches on the main chain, because they are excluded from the lamellae [6, 7]. Branched PE therefore tends to contain thinner lamellae, and hence a more extensive tie-molecule network than linear PE of the same molecular weight [4]. The branch distribution with respect to molecular weight is also important, because branches placed on long molecules (i.e. those most likely to act as tie molecules) are most effective in improving the mechanical properties [8].

Unsurprisingly, the presence of structural features over a range of length scales and the local orientation of molecules and lamellae in different regions of spherulites, result in fairly complex micromechanical behaviour. The molecular and lamellar deformation mechanisms identified in PE have been reviewed by Bowden and Young [9] and Lin and Argon [10]. The influence of microstructure on the mechanical behaviour is important in determining the relative amount of each mechanism, or indeed whether it operates at all. It has been simultaneously investigated on the molecular and lamellar length scales for a wide range of samples and precisely related to the macroscopic response [11–13]. In this paper the deformation response on the spherulitic length scale is investigated, and related to the sample microstructure for the range of samples discussed in previous papers [11–13].

Generally, initial deformation is recoverable and elastic, and is governed by the mechanical properties of the interlamellar amorphous material [10]. The tie

*Author to whom all correspondence should be addressed.

0022–2461

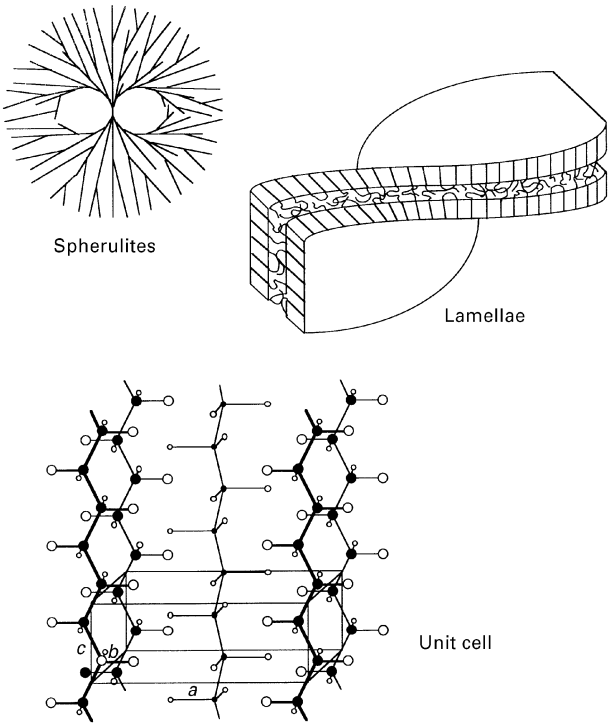

Figure 1 Schematic diagram showing the range of structures in polyethylene, from spherulites to lamellae (shown twisted) to the orthorhombic unit cell.

molecules are particularly important during elastic deformation, because they transmit the stress throughout the structure. Plastic deformation is indicated by the onset of inter- and intraspherulitic yielding, is irrecoverable and results from the slippage of chains and loss of entanglements [9, 10]. The equatorial regions of spherulites, in which the lamellae are disposed favourably to chain slip, usually become extensively deformed, whereas the polar regions, in which the chains are oriented at a large angle to the tensile axis and do not slip so easily, are relatively undamaged. They deform by alternative mechanisms such as twinning and a martensitic transformation from the stable orthorhombic phase to a metastable monoclinic phase, observed only during stress and under 110 °C [9, 10].

Solution casting of films, and their deformation on copper grids, provides a convenient method for the manufacture and investigation of samples for optical and transmission electron microscopy, both of which require sufficiently thin films. Although solution-cast films of amorphous polymers have been extensively studied using the "copper grid technique" [14–19] semicrystalline polymers with a spherulitic morphology have received less attention because of their more complicated microstructure. Nevertheless, the feasibility of such an approach has been demonstrated by several studies, mainly on oriented thin films [20–22], but including some on spherulitic PE, isotactic-polystyrene (PS) and poly(ether ether ketone) (PEEK) [23–26]. Other studies, on melt-crystallized spherulitic thin films have been performed, using a substrate other than a copper grid, which also demonstrate the usefulness of examining pre-deformed thin films [27, 28].

2. Experimental procedure

2.1. Materials and sample preparation

A range of commercial grade high-density polyethylene (HDPE), medium-density polyethylene (MDPE) and linear low-density polyethylene (LLDPE) samples, supplied by BP Chemicals Ltd, was studied in order to investigate the influence of molecular weight, branch type and branch amount on the micromechanical properties of unoriented spherulitic solution-cast thin films. Sample information is summarized in Table I.

Thin films were cast from 3 wt % solutions of PE in xylene. Typically about 4.5 g PE pellets or powder were dissolved in 150 cm^3 hot xylene. A glass slide, cleaned by immersion in concentrated nitric acid for at least 24 h followed by thorough washing with distilled water, was placed in the PE solution. It was left for several minutes in order for the solution and slide temperatures to equilibrate. The slide was then withdrawn at a constant rate. Solution temperatures of 125 and 145 °C, and drawing rates of 1 and 8 cm min^{-1} were used in order to create samples with different thermal histories. These thermal histories will subsequently be referred to as 1:125, 8:125, 1:145 and 8:145. Films were thus produced which had thicknesses, estimated from their appearance (colour) and from ellipsometry measurements of approximately 500–1000 nm.

Once drawn, the glass slides were left in air for 24 h for any residual xylene to evaporate. The film was then cut, using a razor blade, into strips approximately 5 mm wide and 10 mm long which were floated on to the surface of distilled water from the slide. These strips were picked up on electroformed copper grids that had been annealed for 5 h at 520 °C in an argon atmosphere (this annealing is required to encourage ductility of the grids) prior to coating with a thin layer of the same PE grade from a 1 wt % solution (with xylene as solvent). The grids with attached films were then annealed for 1 h in vacuum at 125 °C for HDPE and MDPE samples and 115 °C for LLDPE samples, in order to bond the films to the grids. They were left to cool slowly in vacuum, reaching room temperature after approximately 8 h.

2.2. Deformation

A Rheometrics Ltd Miniature Materials Tester (Minimat) was used to extend the film-bearing copper grid to a fixed extension of 20% strain. Individual squares

TABLE I Sample information

Sample	M_w ($\times 10^3$)	M_w/M_n	SCB[a] ($\times 10^3$C)[b]	SCB type
B	131	6.3	< 0.5	Butyl
C	206	8.6	6.2	Butyl
E	385	9.0	0	–
G	152	5.2	23.7	Ethyl
H	126	4.2	21.0	Iso-butyl
I	110	3.0	~20	Butyl

[a]SCB = short-chain branches. [b]C = carbon atoms on backbone molecule.

were then cut out from the grid using a sharp scalpel for examination using optical and transmission electron microscopy. The copper grid, having deformed plastically, maintained the tension in the film.

The strain-to-deform was measured by extending the copper grid *in situ* during observation with a Jenapol polarizing microscope at ×32 magnification. The extension at which deformation was first observed was recorded. An average was taken from a population of at least eight samples. All deformation was performed at room temperature at a strain rate of $10^{-3}\,s^{-1}$.

2.3. Optical microscopy

A Zeiss Axioplan microscope was used in differential interference contrast (DIC) mode to observe the predeformed samples. Micrographs were taken, with a green filter inserted below the sample, on Ilford 35 mm HP5 film using an Olympus OM10 camera.

2.4. Transmission electron microscopy

A Jeol JEM2000EX transmission electron microscope operating at 200 kV was used to observe the predeformed samples at higher magnifications than could be achieved using optical microscopy, and to obtain selected-area electron diffraction (SAED) patterns. Micrographs were recorded on Kodak "TMax 400" film, chosen for its ability to record low-intensity images (vital for avoiding beam damage to the sample – high-energy electrons rupture C–H and C–C bonds, producing alkyl radicals [29] which combine, with the evolution of hydrogen, to form a cross-link. Cross-linking results in a loss of crystallinity [30–33]. Sample contrast increases during examination and samples change dimensions, with spherulites usually becoming conical). Samples underwent no fixing or staining treatments prior to observation.

The electron beam current was increased to maximum (producing a beam current density of approximately 200 $pA\,cm^{-2}$), and focusing was performed on one part of the sample (which subsequently became extensively damaged). The "lifetime" of the sample, which will be defined as the time for which the diffraction pattern remained unaltered, was a fraction of a second at the full beam current. The current was then reduced until the sample lifetime lay between 10 and 20 s (this was achieved with a beam current density of less than 10 $pA\,cm^{-2}$). The sample was then moved to an undamaged area, but not too far away in order to prevent the need for refocussing, and the film exposed for a time of between 5 and 8 s.

For SAED, a region of the sample of approximately 10 μm diameter was selected by means of an aperture. The beam current was adjusted until a diffraction pattern was obtained from this region that survived for up to 20 s. The sample was then moved to a different area and the film exposed for between 5 and 8 s to record the diffraction pattern. After this the TEM was placed in the imaging mode in order to observe the region from which the diffraction pattern was obtained, although it was usually beam damaged by this time.

3. Results

3.1. Strain-to-deform

Strain-to-deform, (ε_d), values for the different samples are shown in Table II. The following factors increased the strain-to-deform: increasing the drawing rate from solution, increasing the solution temperature, increasing the molecular weight (cf. samples B and E) and increasing short-chain branch density (cf. samples B, C and I). Branch length had no apparent effect. It can be seen that microstructural factors had the greatest influence on ε_d for the 1:125 samples. Although the same trends were observed for the other thermal histories, the differences between the strain-to-deform values were not so great.

3.2. Deformation mechanisms

In all cases, interspherulitic deformation occurred first (marked A in Fig. 2a), with deformation initiating at the nodes where three spherulites met and between short spherulite boundaries (marked B in Fig. 2b) at a well defined strain (given in Table II). Similar behaviour has been observed in spherulitic films of isotactic polystyrene [26]. Following this initial deformation, one of two different spherulitic deformation mechanisms occurred, depending on the sample type. Both of the mechanisms involved deformation between and inside spherulites (inter- and intraspherulitic deformation, respectively).

In the first mechanism, which was observed in the MDPE and LLDPE samples (i.e. the ethylene–α-olefin copolymers) and is shown in the optical micrographs in Fig. 2 for the different 1:125 copolymer films drawn to 20% strain, the spherulites continued to separate by the increasing deformation of their boundaries. Where the interspherulitic deformation met the spherulites, deformation mainly proceeded around rather than through them, although there was a limited amount of deformation inside the spherulite near to the point of meeting. At a strain which was, in some cases, equal to that at which the initial interspherulitic deformation appeared, and in some cases higher than the strain-to-deform, small deformed regions also appeared at several sites around the spherulite centres, marked C in Fig. 2b. These regions became elongated parallel to the tensile axis, but never

TABLE II Strain-to-deform values for the different thermal histories

Sample	Thermal history			
	1:125	8:125	1:145	8:145
B	2.60 ± 0.14	6.14 ± 0.30	6.93 ± 0.62	6.57 ± 0.27
C	3.62 ± 0.18	6.80 ± 0.12	8.57 ± 0.80	8.04 ± 0.31
E	5.85 ± 0.12	7.65 ± 0.13	7.10 ± 0.44	9.68 ± 0.81
G	7.71 ± 0.49	8.54 ± 0.47	–	–
H	7.00 ± 0.21	9.03 ± 0.42	–	–
I	7.53 ± 0.24	10.93 ± 1.40	8.17 ± 0.24	11.33 ± 0.64

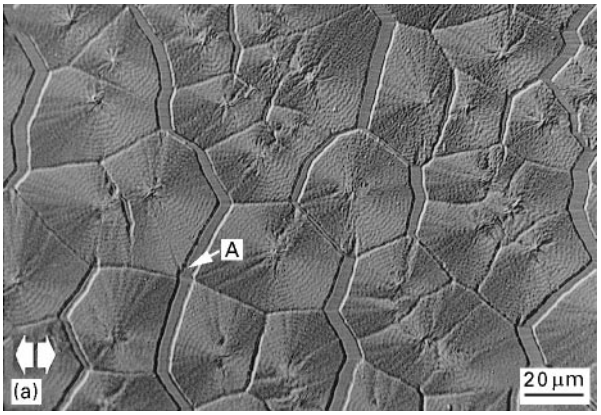

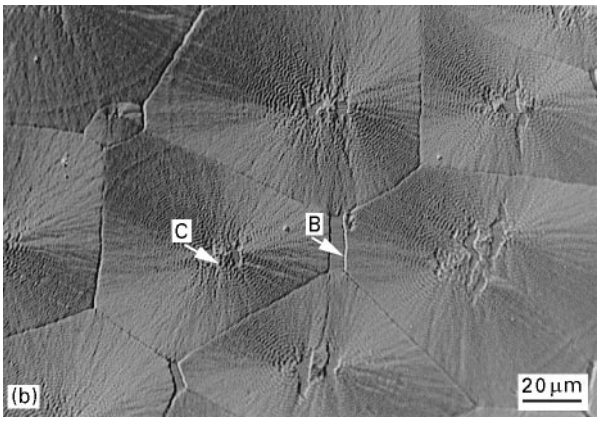

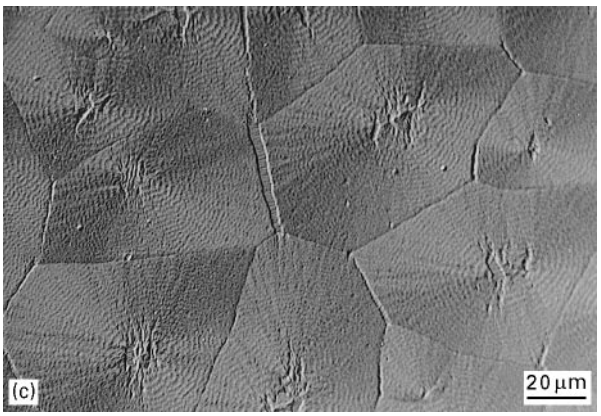

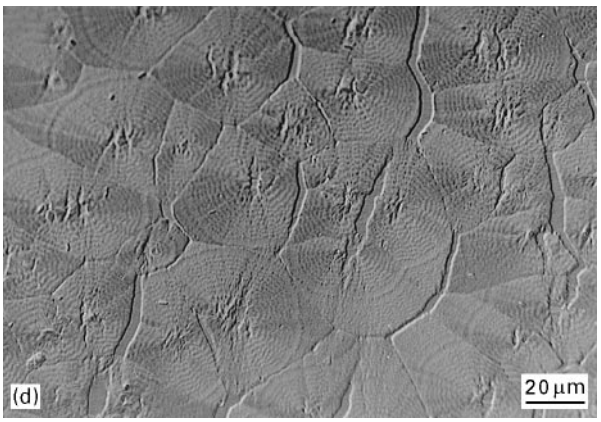

Figure 2 Optical micrographs of the 1:125 MDPE and 1:125 LLDPE samples deformed to 20% strain. (a) Sample C (MDPE), (b) Sample G (LLDPE), (c) Sample H (LLDPE) and (d) Sample I (LLDPE). (a, b) A, Interspherulitic deformation; B, short spherulite boundaries where crazing initiated; C, intraspherulitic deformation. The tensile axis is arrowed.

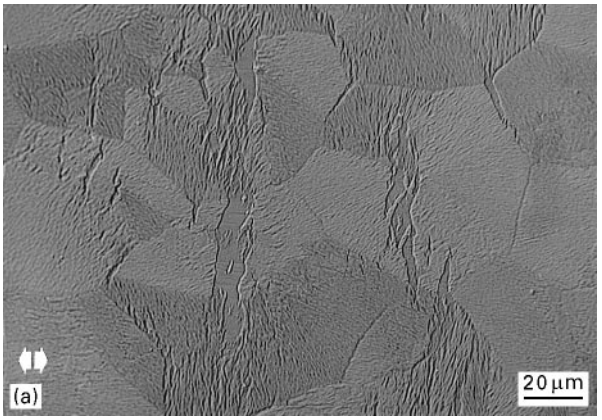

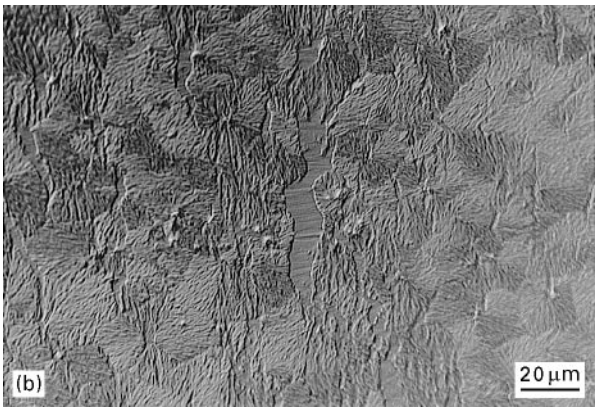

Figure 3 Optical micrographs of (a) HDPE sample B 1:145 and (b) HMW–HDPE sample E 1:145 drawn to 20% strain. The tensile axis is arrowed.

propagated very far laterally into the equatorial regions of the spherulites. There was more interspherulitic deformation in the MDPE sample compared to the LLDPE samples. The results for the LLDPE samples were very similar.

In the second mechanism, observed in the HMW–HDPE and HDPE films (the linear homopolymers), and shown in the optical micrographs in Fig. 3 for both 1:125 homopolymer films drawn to 20% strain, the interspherulitic deformation propagated directly into the spherulites upon meeting them and extensive deformation of the equatorial regions of the spherulites ensued across their entire diameter. It was found that the amount of intralamellar deformation in the higher molecular weight HMW–HDPE sample E, was greater than in the HDPE sample B, for samples with the same thermal history.

For both deformation mechanisms, the specimens drawn more rapidly from solution and from hotter solutions exhibited a greater amount of intraspherulitic deformation. In the copolymers, deformation proceeded almost entirely inside the spherulites for the 8:125 and 8:145 samples. Fig. 4 shows optical micrographs from B 1:145 and B 8:145 showing the greater degree of intraspherulitic deformation in the more rapidly cooled films.

3.3. Deformation microstructure

Optical microscopy cannot reveal the internal morphology of the deformed regions, and so TEM has

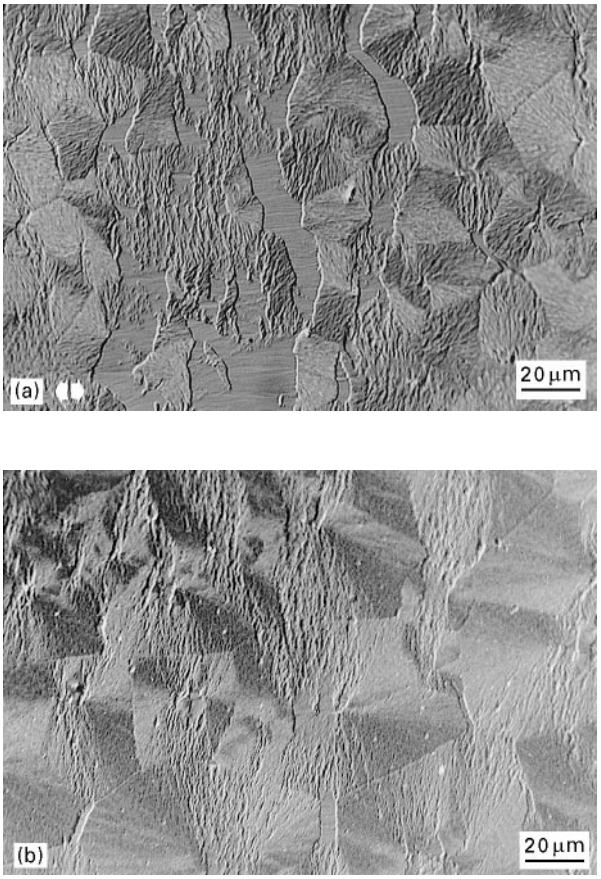

Figure 4 Optical micrographs of (a) HDPE sample B 1:145 and (b) HDPE sample B 8:145 drawn to 20% strain, showing the greater amount of intraspherulitic deformation in the rapidly cooled 8:145 sample. The tensile axis is arrowed.

been used. Fig. 5 shows transmission electron micrographs from interspherulitic deformation for an HDPE (B), MDPE (C) and an LLDPE (H), demonstrating the basic similarity between them. In all cases, the deformed regions consisted of long fibrils spanning the region between the spherulites. However, it can be seen that the fibrils were thicker in the LLDPE sample. Electron diffraction patterns, shown alongside the TEM images in Fig. 5, showed the presence of highly oriented crystalline material in the deformed regions and that a much greater degree of orientation was attained in the HDPE compared with LLDPE. It may be noticed that the monoclinic (0 0 1) reflection (arrowed in Fig. 5b) can also be seen in all cases, indicating the occurrence of the martensitic transformation during deformation. For comparison, Fig. 6 shows a diffraction pattern obtained from a region of an undeformed spherulite (which confirmed that the spherulites in the solution cast films possessed the same radial *b*-axis orientation as in melt-crystallized spherulites).

Intraspherulitic deformation had a different appearance for the different samples. In the LLDPE samples the deformed regions (which were localized near to the spherulite centres) were generally similar in appearance to the interspherulitic deformation, as can be seen in Fig. 7 for sample H 1:125 drawn to 20% strain.

The centre of the micrograph roughly corresponds to the spherulite centre. Note that, owing to the low percentage crystallinity, the contrast (which in a crystalline system results from the crystallinity of the sample) was fairly poor. In the HMW–HDPE and HDPE samples, however, numerous small but extensively fibrillated regions were observed throughout the entire equatorial region of the spherulites. Fig. 8 is a transmission electron micrograph from HDPE sample B 1:145 contrasting the intraspherulitic deformation with the interspherulitic deformation. The fibrillated intraspherulitic regions are arrowed in Fig. 8.

Fig. 9 shows a detail of the intraspherulitic deformation. Entities, arrowed in Fig. 9, with a width of less than 50 nm and often inclined to the tensile axis, were observed in the deformed intraspherulitic regions. Within the spherulites, shown in the transmission electron micrograph in Fig. 10 (from HMW–HDPE sample E8:145), the deformed equatorial regions were permeated with small "islands" of undeformed material. These were recognizable by their similar appearance to the material in samples prior to deformation. SAED showed that, as at the spherulite boundaries, deformed regions within spherulites contained highly oriented crystalline material, both in the obviously fibrillated material in the HDPE and in the deformed regions in the LLDPE, recognizable by their lower contrast. SAED patterns from the deformed intraspherulitic regions were indistinguishable from those

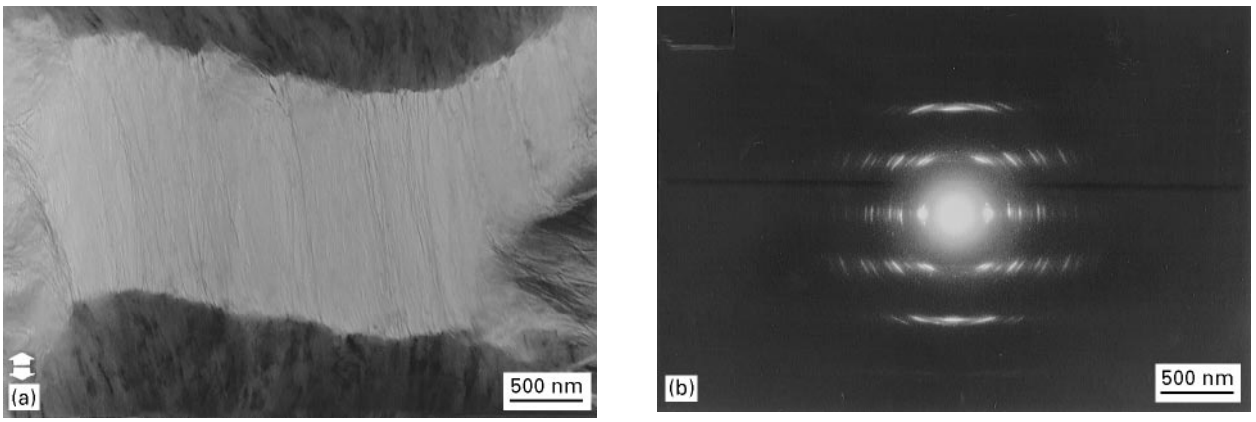

Figure 5 Transmission electron micrographs of (a,c,e) interspherulitic deformation (b,d,f) and the corresponding selected-area electron diffraction patterns for (a,b) HDPE sample B 1:125, (c,d) MDPE sample C 1:125 and (e,f) LLDPE sample H 1:125. The tensile axis is arrowed.

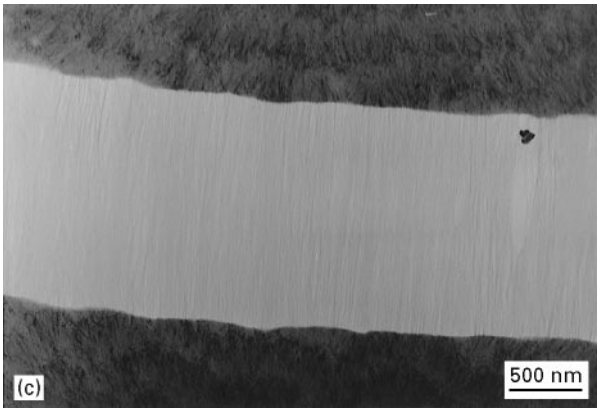

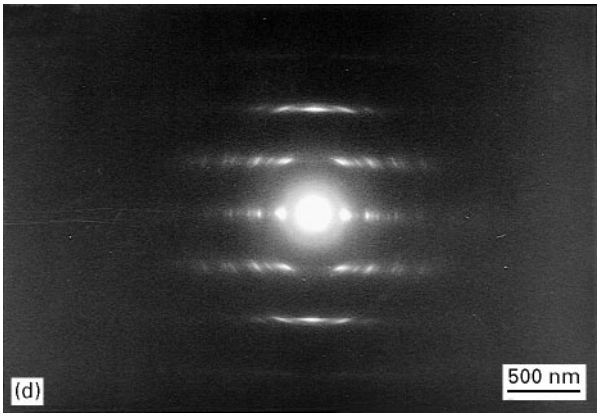

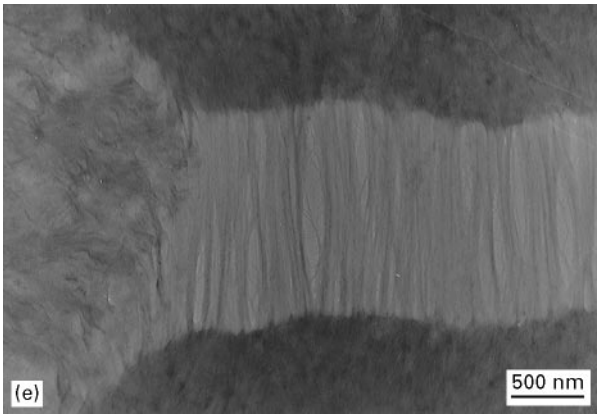

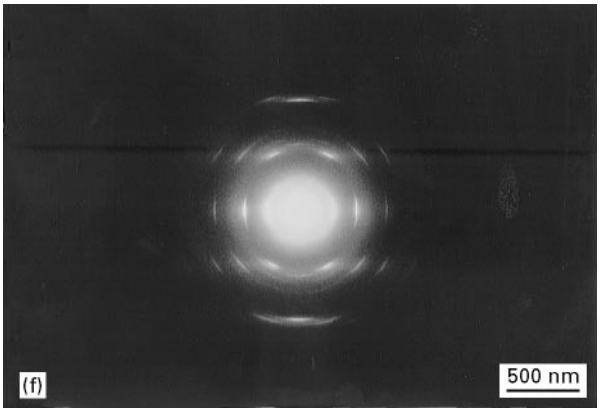

Figure 5 (Continued)

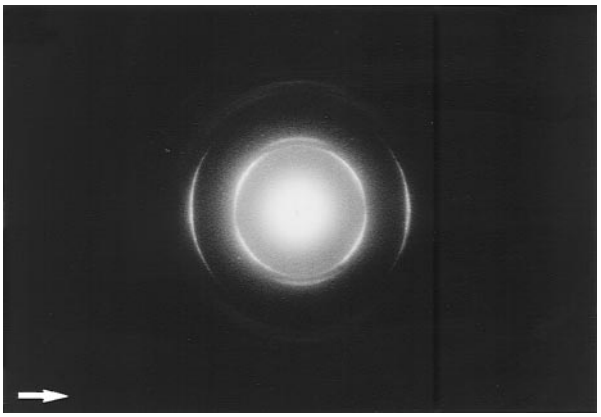

Figure 6 Selected-area electron diffraction pattern from an undeformed spherulite. The direction corresponding to the spherulite radius is arrowed.

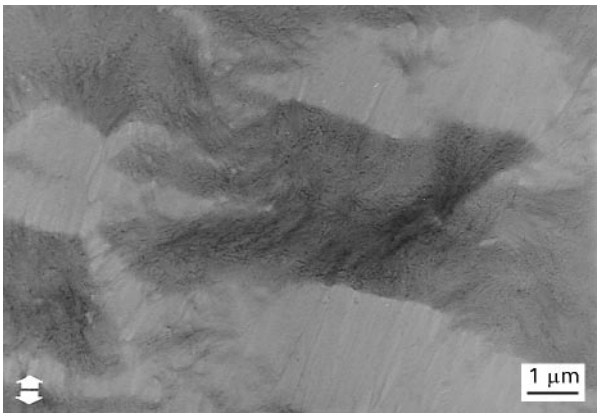

Figure 7 Transmission electron micrograph of intraspherulitic deformation at the spherulite centre (i.e. the regions marked "C" in Fig. 2) in LLDPE sample H 1:125 drawn to 20% strain. The tensile axis is arrowed.

obtained from the interspherulitic regions of the same sample, in all cases.

In order to demonstrate the effect of beam damage, Fig. 11 shows an image from a beam-damaged deformed intraspherulitic region from the HMW–HDPE sample E. Within the deformed area, an oriented stacked lamellar morphology was observed which is not present in samples of the same material observed using a protocol for avoiding beam damage.

4. Discussion

4.1. Strain-to-deform and relation to spherulitic deformation mechanisms

Comparison of the strain-to-deform values with the spherulitic deformation mechanisms leads to the following observation: deformation occurs at higher strains in samples for which intraspherulitic deformation is the dominant spherulitic deformation mode. Any explanation for the strain-to-deform values must therefore take into account the microstructural deformation mode, because the two factors are interlinked. The operative deformation mode must be determined by the relative strengths of the inter- and intraspherulitic regions.

Because the spherulite boundaries always yielded at the strain-to-deform, ε_d, whereas the spherulite interior deformed at a strain greater than or equal to ε_d, it may be supposed that the boundaries are intrinsically weaker. This supposition is not unreasonable,

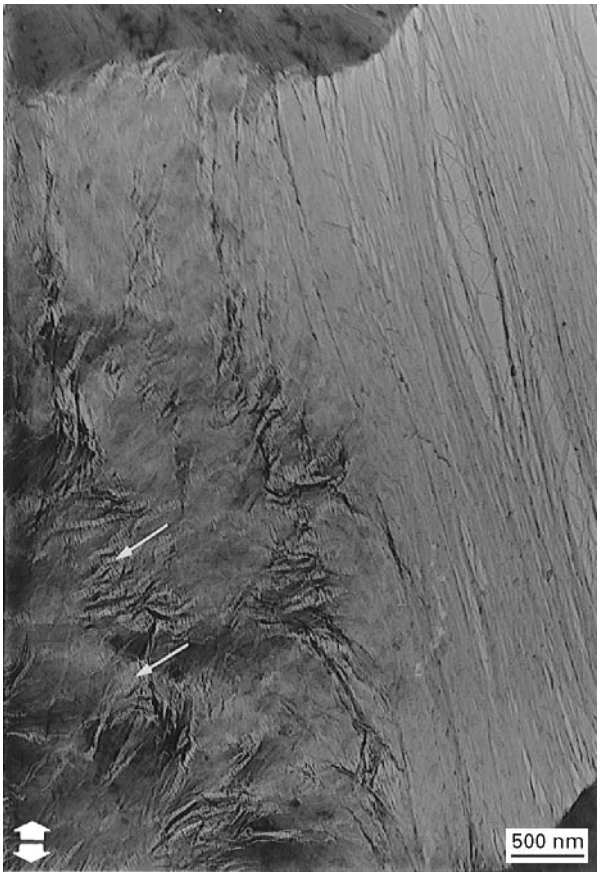

Figure 8 Transmission electron micrograph contrasting inter- and intraspherulitic deformation in HDPE sample B 1:145. The small arrows indicate examples of the small, but numerous, extensively fibrillated regions within the deformed spherulites. The tensile axis is shown by the large arrows.

Figure 9 Detail of the intraspherulitic fibrillated regions indicated in Fig. 8. The dark entities that are indicated by the small arrows are possibly lamellae. The tensile axis is shown by the large arrows.

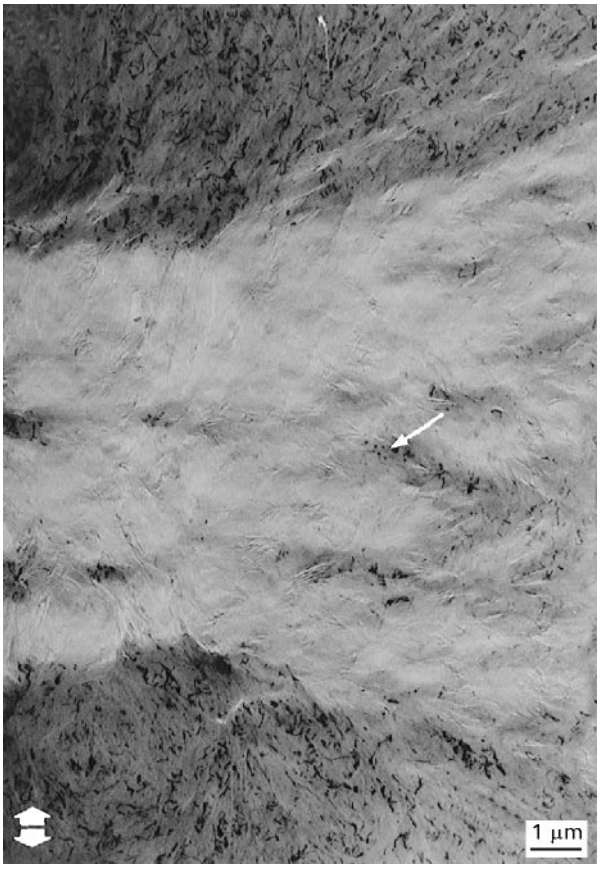

Figure 10 Lower magnification transmission electron micrograph of a deformed equatorial spherulite radius in HMW–HDPE sample E 8:145 drawn to 20% strain. "Islands" of undeformed material are indicated by the small arrows within the intraspherulitic deformation, demonstrating the non-uniform nature of intraspherulitic deformation. The tensile axis is shown by the large arrows.

because interlamellar deformation mechanisms involving the amorphous component are always activated prior to those involving the crystalline lamellae [10]. Because the spherulite boundaries contain the less-perfect material rejected during crystallization, it is reasonable to assume that amorphous deformation mechanisms are more important in interspherulitic deformation than in intraspherulitic deformation [34], where fibrillation may only proceed after lamellar disruption. Indeed, it has been stated previously that the spherulite interiors are stronger than the spherulite boundaries [34].

Therefore, both ε_d and the amount of inter- and intraspherulitic deformation may be altered by modifying the strength of the spherulite boundary relative to the spherulite interior. Increasing the strength of the spherulite boundaries is expected to increase ε_d and increase the amount of intraspherulitic deformation, because a greater degree of deformation must be borne by the (stronger) spherulite interior. Comparison of samples with different thermal histories, molecular weights and branch densities, all of which affect the relative strengths of the inter- and intralamellar regions, provide supporting evidence for the above hypothesis.

Increasing the drawing rate of the slide from solution results in more rapid passage of the crystallizing material through the temperature gradient above the

Figure 11 Transmission electron micrograph of a beam-damaged interspherulitic deformation in HMW–HDPE sample E. An oriented stacked lamellar morphology can clearly be seen within the deformation, with the lamellar normals roughly parallel to the tensile axis (marked by the large arrows).

solution surface. Therefore, the 8:125 and 8:145 films were cooled more rapidly than the 1:125 and 1:145 films, respectively. Shorter crystallization times reduce the amount of fractionation of material, in which shorter molecules, impurities and non-crystallizable chains tend to be rejected to the growth front, and hence to the spherulite boundaries [35]. There will therefore be a greater interspherulitic tie-molecule density in the 8:125 and 8:145 films. An increased tie-molecule density increases the resistance to disentanglement [36], which is a necessary step in the process of plastic deformation for PE [35, 37]. Chain scission, which is an alternative mechanism to disentanglement, may be discounted, because it has been found that PE chains pull out from the crystalline lamellae in preference to breaking [10]. In addition, the thinner lamellae that will form in the less-crystalline 8:125 sample will be able to knit together better at the spherulite boundaries [35]. Therefore, spherulite boundaries in the 8:125 and 8:145 samples will be stronger and less prone to deformation. Strengthening of the spherulite boundaries therefore causes the higher strain-to-deform and greater amount of intraspherulitic deformation observed in the 8:125 and 8:145 films. The different values of ε_d measured between the 1:125 and 1:145 films are thought to result from differences in film thickness. Films prepared from hotter solutions tended to be thicker, and therefore stronger (due to changing stress conditions), accounting for their higher strain-to-deform. They were most probably thicker because the solvent evaporated more rapidly from the glass slide as it was withdrawn from solution, thus depositing a greater amount of polyethylene. It is important to note, however, that the different 1:125 and 1:145 films followed the same trends and that the deformation microstructure, revealed by TEM, was similar for both types of film.

The greater difference between strain-to-deform values for the different 1:125 samples compared to the 8:125 samples may be explained by the chain mobility and the crystallization times in each case. It is suggested that the chain mobilities of the different samples enabled them to manifest their differences only in the 1:125 samples, which crystallized more slowly and would have achieved greater degrees of crystalline perfection and higher percentage crystallinities. In the 8:125 samples the chains, regardless of sample, were not sufficiently mobile to enable them to acquire markedly different conformations from that in solution in the time available for crystallization to occur. Therefore, the different 8:125 samples would be more similar than the different 1:125 samples.

Increasing the molecular weight increases the tie-molecule density [34], resulting in stronger spherulite boundaries. Because the HMW–HDPE film is likely to possess a lower percentage crystallinity (DSC results from bulk samples have demonstrated this for melt-crystallized samples [11–13], and DSC from the initial powder and pellets from which the solutions were made also yielded the same result), it is also likely to possess thinner lamellae than the HDPE film (also demonstrated previously for melt-crystallized samples). Lamellae from adjacent spherulites may then knit together better at the spherulite boundaries [34], as mentioned previously. An increased inter-lamellar tie-molecule density most probably accounts for the smaller amount of inhomogeneous deformation observed in the HMW–HDPE film shown in Fig. 3.

It has been suggested that the short-chain branches present in ethylene–α-olefin copolymers (MDPE and LLDPE) increased the disentanglement resistance in the amorphous component by increasing chain friction [8, 37], thus reducing the chain mobility. Such a situation would increase the strength of the spherulite boundaries (also strengthened by the thinner lamellae at the spherulite boundaries [35]). It is also known that, owing to the exclusion of branches from the crystalline lamellae, there is a greater tie-molecule network and entanglement density throughout the entire structure in LLDPEs [8, 37, 38] compared with HDPE. The overall increase in disentanglement resistance caused by these two factors serves to make the strain-to-deform higher in the copolymer compared with the homopolymer films. Because the disentanglement resistance due to both factors will increase with increasing branch density, the intermediate strain-to-deform behaviour of MDPE, which possessed an intermediate branch density, is expected. Additional evidence for the role of chain mobility in determining the amounts of intra- and interlamellar deformation is provided by the finding of Schultz that at low (sub-ambient) temperatures,

when chain mobility is low, intraspherulitic deformation is dominant [35].

Similar arguments apply when comparing the different behaviour of HDPE and LLDPE as regards deformation within the spherulite. In the HMW–HDPE and HDPE the entire equatorial spherulite diameter deformed, whereas in the LLDPEs only the centres deformed appreciably. There will be a larger interlamellar tie-molecule density in the LLDPE samples. It has previously been found that an increasing interlamellar tie-molecule density causes cracks propagating through spherulites to branch to a greater extent [39]. Increasing the number of tie molecules extends the stress field by transmitting the stress throughout a greater number of lamellae. Therefore a higher strain is required in the LLDPE samples to initiate extensive plastic deformation in the equatorial regions of spherulites. Such sufficiently high strains cannot have been achieved for the LLDPE samples studied, although they were in the HDPE and HMW–HDPE samples. That the intraspherulitic deformation in the LLDPE films initiated around the spherulite centres suggests that they possessed a particular weakness not present in the HDPE of the same molecular weight. Although this weakness can only be speculated upon, it suggests the presence of a larger "defect" at the spherulite centre in the LLDPE which concentrates the stress there.

Finally, branch length and spherulite size were seen to be unimportant. The first finding supports the results for the bulk samples, for which a similar conclusion was drawn. The second finding is concluded from the observation that interspherulitic deformation did not necessarily dominate in the samples containing larger spherulites (compare C 1:125 and I 1:125, in which the latter, which possessed the larger spherulites, deformed to a greater extent inside the spherulites). It has been suggested that, owing to their greater weakness, boundaries of large spherulites should deform to a greater extent [35] but this seems not to be the case. It is generally accepted that microstructural variables, such as percentage crystallinity and lamellar thickness, which are inevitably interlinked with spherulite size, play a greater role in determining PE deformation so that it is misleading to interpret results in terms of spherulite size alone [35, 39].

4.2. Deformation microstructure

The similarity between the transmission electron micrographs showing the interspherulitic deformation for all samples most probably demonstrates a common interspherulitic deformation mechanism. However, the precise details remain uncertain. The highly oriented orthorhombic crystalline material in the fibrils, revealed by electron diffraction, may have originated in lamellae positioned next to the spherulite boundaries that became pulled away as the amorphous material between the spherulites became extended. Alternatively, the amorphous interspherulitic material may have crystallized during deformation. This phenomenon has been observed in the craze fibrils of initially amorphous isotactic polystyrene [40]. An increased entanglement density preventing the separation of material in the amorphous component in LLDPE was indicated by the thicker fibrils observed in that sample [4].

Intraspherulitic deformation is clearly of a different character to the interspherulitic variety. The loss of contrast that is observed in some regions may be due to a reduction in crystallinity decreasing the amount of crystalline diffraction contrast [23]. Thinning of the sample in the deformed region, resulting in insufficient material being available to provide any measurable contrast, may also be the cause. Although the unfolding of chain-folded lamellae has been proposed as the cause of such regions in microtomed sections of drawn bulk LLDPE samples [41], insufficient evidence is available in this case to draw similar conclusions. The identity of the dark areas arrowed in Fig. 9 within the deformed intraspherulitic regions is also unknown. It may be speculated that they are tilted and deformed lamellae, in the orientations that would give rise to four-point SAXS patterns (examples of which have been found in blown films from the same materials [42]). Such structures have previously been imaged both in LLDPE samples [41] and in sections from deformed bulk samples of the same commercial grades studied in this paper [43].

The appearance of the intraspherulitic deformation in the HDPE and HMW–HDPE films is similar to that observed in oriented thin films in which the lamellae were oriented perpendicular to the tensile axis [22] (as they are in the equatorial regions of spherulites). In those studies, deformation initiated at regularly spaced intervals in the amorphous component between the lamellae (giving rise to a regular fibril spacing) [20,34], but during drawing, lamellae disintegrated and were drawn into the fibrils [20,34]. A similar mechanism is proposed to operate in the HDPE and HMW–HDPE films studied in this paper.

Therefore, in intraspherulitic deformation, the lamellae are initially perpendicular to the fibrils into which they are drawn but in interspherulitic deformation they are initially parallel to the fibrils. Two possible deformation mechanisms are that during intraspherulitic deformation, the lamellae disintegrate by coarse slip to allow the incorporation of chain-folded blocks in the fibrils, whereas during interspherulitic deformation, the chains in the lamellae tilt and are then drawn out of the lamellae into the deformed region.

It is likely that the LLDPE samples, in which a high degree of molecular orientation was achieved despite the absence of any identifiable fibrillation, deformed much more homogeneously than the HDPE samples. This result would be in accordance with the X-ray scattering results on deformed bulk samples of the same materials, in which wide-angle X-ray scattering (WAXS) patterns indicated a high degree of molecular orientation whereas small-angle X-ray scattering (SAXS) patterns showed that cavitation did not occur [11,12]. That the intraspherulitic and interspherulitic deformation had a similar appearance in LLDPE but were totally different in HDPE implies that different

deformation mechanisms operated in each case. Possibly, the results may be explicable in terms of some kind of defect at the nucleation site in LLDPE, which reduces the crystallinity of the spherulite centre and causes amorphous deformation mechanisms to operate there as at the spherulite boundaries.

4.3. Beam damage

From the quality of the electron diffraction patterns it can be safely concluded that beam damage was minimal in the time taken to record the images and diffraction patterns, and that the use of fast film with unstained samples has provided a successful method for film examination. Unfortunately, the initial crystalline diffraction contrast has proved unsuitable for the determination of lamellar thickness (a comparison of which before and after deformation would be of interest in addressing the question of whether deformation had occurred by mechanical means or by melting and recrystallization [23]), because it does not reveal lamellar-shaped entities as seen in etched samples. It is concluded that staining and etching techniques would provide the best method for undertaking any quantitative analysis of lamellar thicknesses. The apparent oriented lamellar morphology that was observed in the beam-damaged HMW–HDPE sample bears a similarity to one obtained in a similar study of UHMW–PE [23]. In that case it was concluded that sample heating by the beam had been sufficient to cause melting and recrystallization under stress, but that exposure had stopped short of damaging the crystallinity. A similar explanation may be the case for the HMW–HDPE sample presented in this study.

5. Conclusion

The deformation of spherulitic structures has been shown to be complex, and highly dependent on a number of microstructural variables. Without prior knowledge of these variables the deformation processes cannot be predicted and it is therefore impossible to generalize any results to all PE samples. However, it has been shown that spherulite boundaries are the weakest regions of spherulitic structures in PE and that higher strains are generally required to deform the interiors of spherulites, which deform by a different mechanism. Methods for increasing the toughness of the films primarily involve increasing the tie-molecule density and disentanglement resistance to strengthen spherulite boundaries. Three methods for achieving this objective have been demonstrated: (a) decreasing the crystallization time in order to increase the tie-molecule density, (b) increasing the molecular weight in order to increase the tie-molecule density, and (c) incorporating short-chain branches on the main chains in order to increase the tie-molecule density and increase the disentanglement resistance. Incorporation of short-chain branches was shown to be the most effective way of strengthening spherulitic structures, with the toughest films being those made of branched PE that had been crystallized rapidly. It may be conjectured that a high molecular weight, rapidly cooled, branched PE would show an even greater improvement. The branch length and spherulite size were found to be unimportant.

Acknowledgements

The help of the following people is gratefully acknowledged: Dr Elinor Kerr (BP Chemicals Ltd) for supplying the samples, and Roger Peck (Cavendish Laboratory, University of Cambridge) for help with setting up the solution-casting apparatus. The advice of Dr Carrie Walsh regarding the use of the TEM and fast EM film was greatly appreciated. The financial support of the EPSRC and BP Chemicals is acknowledged.

References

1. C. W. BUNN, *Trans. Farad. Soc.* **35** (1939) 482.
2. B. WUNDERLICH, "Macromolecular Physics", Vol. 1 (Academic Press, New York, 1973).
3. H. D. KEITH and F. J. PADDEN Jr, *J. Polym. Sci.* **41** (1959) 525.
4. Y.-L. HUANG and N. BROWN, *J. Polym. Sci. Polym. Phys. Edn* **29** (1991) 129.
5. J. D. HOFFMAN, G. T. DAVIS and J. I. LAURITZEN Jr, in "Treatise on Solid State Chemistry", Vol. 3 edited by N. B. Hannay (Academic Press, New York, 1973) pp. 447–694.
6. P. J. PHILLIPS, *Rep. Prog. Phys.* **53** (1990) 549.
7. W. S. LAMBERT and P. J. PHILLIPS, *Macromolecules* **27** (1994) 3537.
8. Z. ZHOU and N. BROWN, *Polymer* **35** (1994) 3619.
9. P. B. BOWDEN and R. J. YOUNG, *J. Mater. Sci.* **9** (1974) 2034.
10. L. LIN and A. S. ARGON, *ibid.* **29** (1994) 294.
11. M. F. BUTLER, A. M. DONALD, W. BRAS, G. E. DERBYSHIRE, G. R. MANT and A. J. RYAN, *Macromolecules* **28** (1995) 6383.
12. M. F. BUTLER, A. M. DONALD and A. J. RYAN, *Polymer* accepted.
13. *Idem*, *ibid.*
14. B. D. LAUTERWASSER and E. J. KRAMER, *Philos. Mag. A* **39** (1979) 469.
15. E. J. KRAMER, *Adv, Polym. Sci.* **52** (1983) 1.
16. C. J. HENKEE and E. J. KRAMER, *J. Polym. Phys. Polym. Phys. Edn* **22** (1985) 727.
17. A. M. DONALD, *J. Mater Sci.* **20** (1985) 2630.
18. L. L. BERGER and E. J. KRAMER, *Macromolecules* **20** (1987) 1980.
19. C. J. G. PLUMMER and A. M. DONALD, *J. Polym. Sci. Polym. Phys. Edn* **27** (1989) 327.
20. W. W. ADAMS, D. YANG and E. L. THOMAS, *J. Mater. Sci.* **21** (1986) 2239.
21. J. M. BRADY and E. L. THOMAS, *ibid.* **24** (1989) 3311.
22. *Idem*, *ibid.* **24** (1989) 3319.
23. H.-J. KESTENBACH and J. PETERMANN, *Polymer* **35** (1994) 5217.
24. C. J. G. PLUMMER and H.-H. KAUSCH, *ibid.* **34** (1993) 305.
25. *Idem*, *ibid.* **34** (1993) 1972.
26. D. E. MOREL and D. T. GRUBB, *ibid.* **25** (1984) 417.
27. P. ALLAN and M. BEVIS, *Philos. Mag.* **35** (1977) 405.
28. *Idem*, *ibid.* **41** (1980) 555.
29. A. KELLER, in "Developments in Crystalline Polymers" vol. 1 edited by D. C. Bassett (Applied Science London, 1982) pp. 37–114.
30. E. L. THOMAS, in "Structure of Crystalline Polymers" edited by I. H. Hall (Elsevier, London, 1984) pp. 79–124.
31. D. T. GRUBB, A. KELLER and G. W. GROVES, *J. Mater. Sci.* **7** (1972) 131.

32. D. T. GRUBB and A. KELLER, *ibid*. **7** (1972) 822.
33. D. T. GRUBB, *ibid*. **9** (1974) 1715.
34. K. FRIEDRICH, *Adv. Polym. Sci.* **52** (1983) 225.
35. J. M. SCHULTZ, *Polym. Eng. Sci.* **24** (1984) 770.
36. X. LU and N. BROWN, *Polymer* **28** (1987) 1505.
37. N. BROWN and Z. ZHOU, *Macromolecules* **28** (1995) 1807.
38. Z. ZHOU, X. LU and N. BROWN, *Polymer* **34** (1993) 2520.
39. J. H. YEH and J. RUNT, *J. Polym. Sci. Polym. Phys. Edn* **29** (1991) 371.
40. D. E. MOREL and D. T. GRUBB, *J. Mater. Sci. Lett*. **3** (1984) 5.
41. M. FURATA and K. KOJIMA, *J. Macromol. Sci. Phys.* **B25** (1986) 349.
42. M. F. BUTLER, A. M. DONALD and A. J. RYAN, *J. Appl. Polym. Sci*., submitted.
43. M. E. VICKERS, *private communication* (1996).

Received 10 December 1996
and accepted 10 February 1997